ACS Catalysis

Research Article

pubs.acs.org/acscatalysis

Activation of Aryl Chlorides in Water under Phase-Transfer Agent-Free and Ligand-Free Suzuki Coupling by Heterogeneous Palladium Supported on Hybrid Mesoporous Carbon

Linlin Duan,[†] Rao Fu,[†] Zhiguang Xiao,[†] Qingfei Zhao,[†] Jian-Qiang Wang,[‡] Shangjun Chen,[†] and Ying Wan*[,†]

[†]Key Laboratory of Resource Chemistry of Ministry of Education, Shanghai Key Laboratory of Rare Earth Functional Materials, and Department of Chemistry, Shanghai Normal University, Shanghai 200234, P. R. China

[‡]Shanghai Synchrotron Radiation Facility (SSRF), Shanghai Institute of Applied Physics, Chinese Academy of Sciences, Shanghai, 201204, P. R. China

Supporting Information

ABSTRACT: In this study, heterogeneous palladium catalysts supported on ordered mesoporous cobalt oxide−carbon nanocomposites were applied to the water-mediated Suzuki coupling reaction of chlorobenzene and phenylboronic acid and exhibited a high yield of biphenyl (49%) under mild reaction conditions free of phase-transfer agents and ligands. Product yields in the reaction of aryl chlorides containing electron-withdrawing groups attached to their benzene ring can reach approximately 90%. Thiol-functionalized mesoporous silica, which can trap soluble Pd species, was used to confirm the negligible leaching in solution and therefore heterogeneous reaction. This heterogeneous catalyst is stable, showing unobvious activity loss after 10 catalytic runs. Characterization by X-ray diffraction, transmission electron microscopy, X-ray photoelectron spectroscopy, X-ray absorption fine structure analysis, and N_2 sorption techniques revealed intercalated CoO nanoparticles inside a carbon matrix with uniform mesopore sizes (~3 nm), high surface area (~504 m^2/g), and large pore volumes (~0.38 cm^3/g). Additionally, very small Pd clusters consisting of approximately three atoms and Pd−O bonds formed on the interface between CoO and Pd nanoparticles. The unsaturated coordinative Pd may be responsible for the activation of chlorobenzene in the absence of any additives or ligands. Uniform mesopores and the hydrophobic nature of the carbon support may also facilitate the mass transfer of the reactant molecules and enrichment inside pores. For comparison, the catalytic activities of Pd catalysts supported on pristine mesoporous carbon and carbon embedded with nickel oxide nanoparticles were also tested.

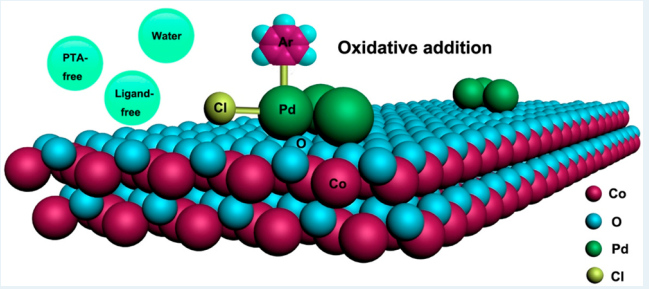

KEYWORDS: *Pd cluster, hybrid mesoporous carbon, aryl chloride, Suzuki coupling, water, TBAB-free, ligand-free*

1. INTRODUCTION

Palladium-catalyzed Suzuki coupling reactions that lead to the formation of new C−C bonds are of strategic importance in synthetic organic chemistry because of the broad functional group tolerance of this catalytic process, its mild reaction conditions, and the stability and low toxicity of the boronic acids employed.[1] Aryl bromides, iodides, and triflates have been extensively investigated for use as substrates in the reaction, as they are easily activated by active Pd(0) species.[2] However, aryl chlorides, which are more economical and accessible than the previously mentioned species, have rarely been used as electrophiles in Pd-catalyzed Suzuki coupling due to the high activation barriers associated with the difficult oxidative insertion of Pd(0) species into the Ar−Cl bond.[3]

The reaction of aryl chlorides in Suzuki coupling has been made possible due to the improved understanding of the reaction mechanism and of the methods for overcoming the rate-determining oxidative insertion step.[3a,b,4] Understanding the properties of the Pd intermediates in the catalytic cycle has allowed the reaction to be performed using a wider range of substrates, with improved selectivity under milder conditions.[5] A large amount of studies have focused primarily on designing electron-rich catalytic sites on homogeneous catalysts by introducing special and costly ligands, such as sterically hindered and electron-rich phosphanes and N-heterocyclic carbenes or palladacycles,[6] that facilitate activation of the C−Cl bond. However, the contamination of the products by Pd residues even after the purification step poses an acute problem, particularly for the pharmaceutical industry.[7] Ligand-free heterogeneous Pd-based catalysts have attracted much attention because they possess great advantages in terms of recyclability. Such catalysts include metallic Pd nanoparticles (NPs)

Received: September 8, 2014
Revised: November 9, 2014

DOI: 10.1021/cs501356h
ACS Catal. 2015, 5, 575−586

supported on silica,[8] zeolites,[9] carbon nanotubes,[10] graphite oxide and graphene,[11] polymers,[12] metal organic frameworks,[3c,13] and oxides.[14] Among these catalysts, Pd/C has been found to act as an efficient alternative to the usual homogeneous conditions.[15] Buchecker and co-workers developed the Pd/C-catalyzed Suzuki reaction in organic solvents under nitrogen.[16] Since then, ligand-free Pd protocols that catalyze Suzuki cross-coupling with aryl chlorides have been developed and are attracting an increasing amount of attention. Sun, Sowa, and co-workers reported the high-yield cross-coupling reaction of electron-poor aryl chlorides with phenylboronic acid when catalyzed by 5% Pd/C (5 mol %) using the very polar solvent dimethylacetamide (DMA) with a small amount of water. Electron-rich, nonactivated aryl chlorides can also react, albeit with much lower yields.[17] Additives used to enhance the catalytic activity of Pd/C would address this issue. Lysén and Köhler reported exceptional enhancement of the catalytic activity of Pd(II)/C by tetrabutylammonium bromide ($(C_4H_9)_4N^+Br^-$, TBAB) in water.[18] TBAB has been proven to be an efficient additive for activating aryl chlorides using a variety of supported Pd nanoparticle catalysts, while the long-chain surfactant cetyltrimethylammonium bromide (CTAB) is not.[19,20] This result implies that the positive effect of TBAB cannot be solely attributed to being a phase-transfer agent. A relatively high temperature (100−140 °C) in water may favor the precipitation of colloidal Pd nanoparticles that can be stabilized by $R_4N^+X^-$.[7,21] Even at a relatively mild conditions (65 °C) in water, bromide ions enhance the dissolution of active Pd species and stabilize these species in solution. The leaching Pd species can redeposit on the solid at the end of the reaction, and noticeably, this process shows a minor effect on metal distribution in some cases.[19,20] Tetrabutylammonium ions also provide activating counterions for the boronate and palladate species and work as a phase-transfer agent. As a result, the possibility of leaching catalytically active palladium colloid species into solution cannot be ruled out, and the enhancement of TBAB to the catalyst activity implies that the reaction takes place in the solution phase.[20]

A heterogeneous, surfactant-free and ligand-free Pd-catalyzed carbon−carbon cross-coupling reaction system that utilizes less expensive chlorobenzene compounds in an aqueous environment offers the environmental benefits of using water instead of dipolar aprotic organic solvents. In addition, this system offers the advantages of easy catalyst recycling and negligible contamination of the products by Pd residues. Although homogeneous Pd-containing catalysts electron-enriched by the introduction of special ligands can activate aryl chlorides, the activity of heterogeneous Pd NP-based catalysts can also be enhanced by modifying their electron density via support effects. However, approaches for significantly improving heterogeneous Pd NP catalysts are still rare; the electron density within the metal has previously been difficult to modify on the nanoscale.[12,22] This problem is much more serious with the presence of the conventional activated carbon supports. The functionalization of the support, which is an efficient method for modifying the electronic chemistry of the supported metal, is always limited by the poor controllability of activated carbon due to its inert surface.[23] In addition, many examples of significant Pd leaching have been reported.[22a] This drawback greatly limits the applications of carbon-supported Pd catalysts. Recently, we found that embedding inert silica into the mesoporous carbon matrix serves to stabilize the Pd nanoparticles. The 3.5 nm Pd NPs facilitate the activation of chlorobenzene in water.[24] A further enhancement of the activity of heterogeneous Pd NP-based catalysts can be attained by modifying their electron density by incorporating intercalated transition metal oxide nanoparticles in the carbon matrix. In this work, we found that such transition metal oxide nanoparticles, which have high crystallinity and can be intercalated into carbon mesopore systems,[25,26] can significantly modify the electron density and dispersion of Pd nanoparticles through metal oxide interfacial interactions. Very small Pd clusters of approximately three atoms are formed. These clusters favor the activation of chlorobenzene in the absence of TBAB and ligands. The mesoporous Pd/CoO−C catalyst exhibits a high yield of biphenyl (49%). When chlorobenzene derivatives with aromatic electron-withdrawing groups are employed in the reaction, the product yields are as high as 90%. The heterogeneous nature of the catalysis was shown by the negligible activity loss in the presence of a trapping agent of thiol-functionalized mesoporous silica added at an SH/Pd ratio of approximately 35. This catalyst is stable, showing negligible metal leaching and activity loss after 10 catalytic runs. The reusability and good activity of the Pd/CoO−C catalyst and its ability to function with additives (such as TBAB) or ligands offer good opportunities for practical applications in coupling reactions and hydrogenation.

2. EXPERIMENTAL SECTION

2.1. Catalyst Preparation. The ordered mesoporous oxide−carbon composite supports were synthesized using $Co(NO_3)_2{\cdot}6H_2O$ or $Ni(NO_3)_2{\cdot}6H_2O$ as metal sources, low-polymerized phenolic resins (preparation described in the Supporting Information, SI) as the carbon source, and triblock copolymer P123 as a structure-directing agent. In a typical synthesis of mesoporous CoO−C, 0.5 g of triblock copolymer P123 was dissolved in 10.0 g of ethanol while stirring at 40 °C until the solution was clear. Then, 0.125 g of $Co(NO_3)_2{\cdot}6H_2O$ was added to the solution, which was stirred for an additional 30 min. Then, 5.0 g of 20 wt % phenolic resin ethanolic solution was added, and stirring continued for another 10 min. The mixture was transferred into multiple dishes. These dishes were then placed in a hood to evaporate the ethanol at room temperature for 5−8 h and were subsequently placed in an oven to thermopolymerize the Bakelite at 80 °C for 24 h. The as-made transparent films were scraped from the dishes, ground into fine powders, placed in a quartz boat, and put in a tubular oven. The powders were calcined at 600 °C in high-purity nitrogen (99.99 vol %) for 6 h to remove the triblock copolymer templates, carbonize the matrix, and decompose the transition oxide. The transition metal oxide content in the catalyst was determined by inductively coupled plasma atomic emission spectroscopy (ICP-AES). The synthesis is easily duplicated. The syntheses of the mesoporous NiO−C and carbon (MC) materials were performed as described by the references in the SI.[25,27] Supported palladium catalysts were prepared by isochoric impregnation. In a typical procedure, 1.7 g of an aqueous solution of $PdCl_2$ (1.1 wt %) was impregnated with 0.4 g of dry mesoporous carrier. The mixture was placed in a hood overnight. The catalysts were then dried at 100 °C under vacuum for 8 h, reduced at 200 °C in forming gas (10 vol % H_2 in nitrogen) for 3 h, and used as fresh supported catalysts (Pd/CoO−C, Pd/NiO−C, and Pd/MC).

2.2. Characterization. X-ray diffraction (XRD) measurements were obtained on a Rigaku Dmax-3C diffractometer using Cu Kα radiation (40 kV, 30 mA, λ = 0.15408 nm). The d

DOI: 10.1021/cs501356h
ACS Catal. 2015, 5, 575−586

spacing values were calculated by the formula $d = \lambda/2 \sin\theta$, and the unit cell parameters were calculated from the formula $a_0 = 2d_{10}/\sqrt{3}$. The metallic Pd sizes were estimated according to the Scherrer formula: size = $0.89\lambda/\beta \cos\theta$ on the basis of the (111) diffraction peak in the wide-angle XRD patterns. CO chemisorption was conducted on a Quantachrome CHEM-BET-3000 system by pulsing CO on the supported Pd catalyst. Palladium nanoparticle sizes were calculated from CO pulse chemisorption data assuming that all palladium particles were spherical and that the adsorption stoichiometry was one CO molecule per Pd atom.[28] CO adsorption was assumed to be complete after three successive peaks showed the same peak areas. High-resolution scanning electron microscopy (HRSEM) images were taken on a JEOL JSM 6380LV microscope operated at 25 kV. Transmission electron microscopy (TEM) experiments were conducted on a JEM 2100 microscope operated at 200 kV. The samples for TEM measurements were suspended in ethanol and supported on a holey carbon film on a Cu grid. Energy-dispersive X-ray spectroscopy (EDX) was performed on a Philips EDAX instrument. X-ray photoelectron spectroscopy (XPS) measurements were performed on a PerkinElmer PHI 5000CESCA system with a base pressure of 10^{-9} Torr. The metal ion concentrations were quantified using ICP-AES (VISTA-MPX). The X-ray absorption spectroscopy data were collected on Beamline BL14W1 at the Shanghai Synchrotron Radiation Facility (SSRF). The electron storage ring was operated at 3.5 GeV, and a double Si(311) crystal monochromator was employed for energy selection. XAS data of the samples were acquired in fluorescence mode using a 32-element Ge solid-state detector. XAS data of standard samples, including Pd foil and PdO, were also measured under similar conditions for comparison. XAS data analysis was performed using the Ifeffit software package.[29] Standard procedures were followed to analyze the XAS data. First, the raw absorption spectrum in the pre-edge region was fitted to a straight line, and the background above the edge was fitted with a cubic spline. The EXAFS function, $\chi(E)$, was obtained by subtracting the post-edge background from the overall absorption and then normalized with respect to the edge jump step. The normalized $\chi(E)$ was transformed from energy space to k space, where k is the photoelectron wave vector. The $\chi(k)$ data were multiplied by k^2 as a weighting factor to compensate for the damping of EXAFS oscillations in the high k region. The range of the k space used for Fourier transformation (FT) is 3.2−12 Å, and the range of the r space used for the curve fitting of EXAFS data is 1−3 Å. The backscattering amplitude and the phase shift were obtained by theoretical calculation using FEFF code (version 6.0).[30] An S_0^2 value of 0.7 was obtained from fitting PdO. From the analysis, structural parameters such as the coordination number (N), bond distance (R), Debye−Waller factor (σ^2), and inner potential shift (ΔE_0) were calculated for the Pd component of each sample. N_2 adsorption−desorption isotherms were measured at 77 K with a Micromeritics Tristar II 3020 analyzer. The Brunauer−Emmett−Teller (BET) method was utilized to calculate the specific surface areas (S_{BET}) of the samples. By using the Barrett−Joyner−Halenda (BJH) model, the pore volumes and pore size distributions were derived from the adsorption branches of isotherms.

2.3. Catalytic Reactions. Suzuki cross-coupling reactions were conducted in a 50 mL round-bottomed flask under refluxing conditions with water as the solvent. Typically, 2 mmol of sodium carbonate (K_2CO_3) was dissolved in 10 mL of water and placed in the reactor. To this solution were added 0.03 g of supported palladium catalyst containing 0.01 mmol metallic Pd and 1.0 mmol of chlorobenzene, and the mixture was heated to 80 °C. Finally, 1.2 mmol of phenylboronic acid was added to start the coupling reaction. The products of the reaction were centrifuged, extracted with ethyl acetate or toluene, and analyzed. At different time intervals, hot filtration was used to determine the degree of Pd leaching and chlorobenzene conversion.[31] The catalyst was separated and submitted to continuous solid−liquid extraction with ethyl acetate or toluene (5 mL) using micro-Soxhlet equipment. Then, the solid catalyst was washed with a copious amount of water and dried at 80 °C overnight under vacuum for reuse. The extracted solution was mixed with the reaction solution, and the mixture was extracted with ethyl acetate (10 mL). The solids obtained were weighed and analyzed. The recovered material accounted for more than 95% of the starting material. About 98% carbon balance can be established between chlorobenzene and biphenyl with the error of 5%. The coupling reaction was repeated three times, yielding the same initial rates and total conversion within ±10%. To identify and analyze the products, GC−MS equipped with a JW DB-5 capillary column was used. Standard samples of each chemical were also analyzed for comparison. The analysis was repeated at least three times for all tests, and the experimental errors were within ±5%. Catalytic results are presented in terms of the absolute yield of biphenyl, the conversion of chlorobenzene, the initial rate (mmol of reacted chlorobenzene per mmol of Pd per hour) calculated at the beginning of the reaction and the turnover number (TON, mmol of reacted chlorobenzene/total Pd concentration).[32] The products were also isolated and purified by column chromatography. The isolated components were identified by ^{1}H NMR analysis on a Bruker DRX 400 spectrometer, using tetramethylsilane as the internal standard. The aqueous solution was collected to determine the Pd leaching concentration. In reactions in which homogeneous palladium acetate was used as the (pre)catalyst, 2 mmol of TBAB was added before the preheating step, and the reaction was initiated by adding 0.01 mmol of palladium acetate in water.

For the soluble Pd trapping experiments, we followed the method reported by Jones and co-workers using thiol-group-modified mesoporous silica (SH-SBA-15).[33] The preparation and characterization of SH-SBA-15 are described in the SI (Figures S1−S5). In standard experiments, 0.15 g of SH-SBA-15 was added to the reaction flask before the addition of the reaction solution (with a molar ratio of SH/Pd = ∼35:1).

For the recycling study, the Suzuki reaction was performed with chlorobenzene and phenyl boronic acid, maintaining the same reaction conditions as described above except using recovered catalyst. After each completion of the reaction, the catalyst was recovered by hot filtration and thoroughly washed with ethyl acetate followed by a copious amount of water to remove the organic and inorganic impurities from the used catalyst. The recovered catalyst was dried under vacuum at 80 °C overnight, weighed, and reused in the next run. Several parallel reactions were performed to ensure that the catalyst amount was the same in each run. The palladium content of the solid was measured at the first and the last reuses.

3. RESULTS AND DISCUSSION

3.1. Composition and Structure of Supported Palladium Mesoporous Catalysts. The syntheses of mesoporous carriers used a metal-containing lyotropic liquid-crystal self-

DOI: 10.1021/cs501356h
ACS Catal. 2015, 5, 575−586

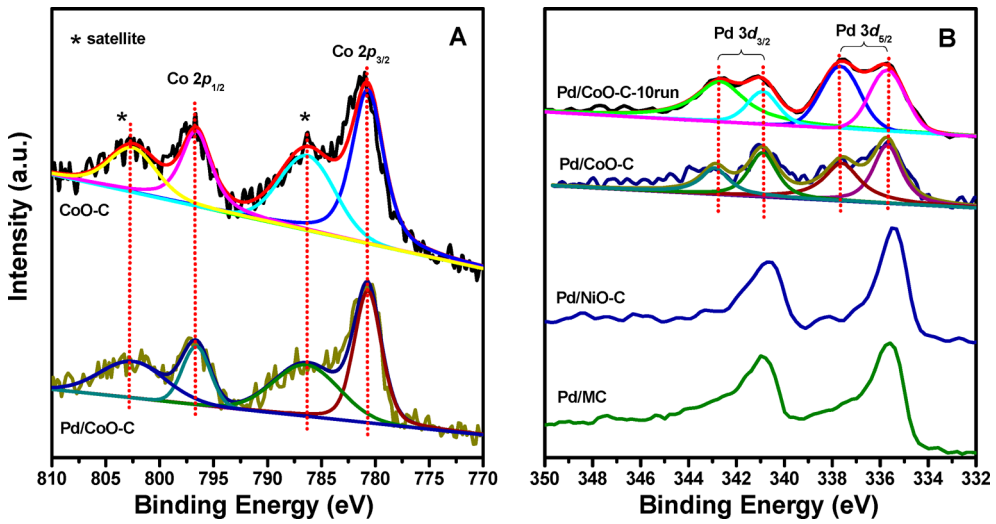

Figure 1. XPS spectra in the (A) Co 2p and (B) Pd 3d regions for the mesoporous carrier, fresh supported Pd catalyst, and used Pd catalyst.

assembly route with hydrated nitrate salt as a metal source, soluble phenolic resin as a carbon source, and triblock copolymer as a structure-directing agent.[25,26] The wide-angle XRD patterns for the mesoporous CoO−C carrier display crystalline peaks that can be matched to the series of Bragg reflections corresponding to the pure cubic rock salt structure of CoO (*Fm*3*m*, JCPDS: 65-2901, SI Figure S6). The oxide particle size, estimated from the Scherrer formula, is approximately 5 nm (the size perpendicular to the 111 plane), and the Co content, estimated from ICP-AES analysis, is approximately 5.8 wt %. The XPS spectrum of the CoO−C carrier in the Co 2p region (Figure 1A) shows peaks at 780.7 eV due to Co $2p_{3/2}$ (with a shakeup satellite at 786.4 eV) and at 796.7 eV due to Co $2p_{1/2}$ (with a satellite peak at 802.7 eV).[34] The Co^{2+} cations in CoO are high-spin d^8 and in octahedral lattice sites. The intense satellite structure has been proposed to result from the charge-transfer band structure found in late 3d transition metal monoxides with partially filled e_g character and is commonly used to identify cobalt-containing oxides as the rock salt monoxide.[35] Therefore, this cobalt oxide is consistent with the presence of Co^{2+} in the high-spin state. The absence of a feature at 778.1 eV indicates the absence of Co metal impurity.[35b] The formation of low chemical state transition metal oxide in a mesoporous oxide−carbon composite has also been confirmed for MnO−C.[26] It should be mentioned that the peak intensities of the CoO−C carrier are rather low, demonstrating that the surface and near-surface concentrations of Co are far below the concentration in the bulk material. These results indicate that the transition metal oxide nanoparticles are embedded in the carbon pore system, similar to the structure of mesoporous MnO−C, with a low chemical state and coordinative unsaturation.[26] The NiO−C carrier exhibits several diffraction peaks, which can be indexed to the (111), (200), and (220) planes of face-centered cubic (fcc) NiO (*Fm*3*m*, JCPDS: 65-2901, SI Figure S6), as reported in the literature.[25] The NiO particle size is calculated to be 9.0 nm, and the content is 7.2 wt %. The diffused diffraction peaks at approximately 20° for all mesoporous carriers can be attributed to the amorphous carbonaceous materials.

After incorporation of the Pd species, the XPS spectrum (Figure 1B) of Pd/NiO−C shows characteristic binding energies of Pd $3d_{3/2}$ and $3d_{5/2}$ in metallic Pd species, similar to Pd supported on pristine mesoporous carbon.[36] In addition, the involvement of CoO inside the carbon matrix shows a significant effect on the Pd chemical state. The Pd $3d_{3/2}$ and $3d_{5/2}$ peaks for Pd/CoO−C can be fitted using a model consisting of two peaks, where the peaks corresponding to Pd(0) are at 340.9 and 335.7 eV, and the peaks of Pd−O are at 342.7 and 337.7 eV.[37] At the same time, the features in the Co 2p region for cobalt monoxide can be maintained. The strong electronic interactions of the catalyst with the support are thought to be the predominant cause of the effect on the electronic structure of the active particle.[38] The electronic changes are often specifically attributed to interface sites between the particle and the support.[39] The formation of a thin Pd−O layer at the interface between Pd and transition oxide Fe_3O_4 support has been investigated by Libuda and coworkers.[38] The interface oxide layer, which is stabilized by the support, is capable of oxygen exchange with both the metallic Pd surface and Fe_3O_4, showing complex and low kinetics, respectively. Therefore, the interaction between Pd and low-oxidation-state CoO may lead to the formation of a PdO layer at the Pd/CoO−C interface.

The *K*-edge XANES was used to probe the electronic transition from the 1s to 5p Pd orbitals and is sensitive to the chemical state of the sample. The pre-edge line in the Pd *K*-edge XANES spectrum of the Pd/NiO−C catalyst shows a strong resemblance to the reference spectrum of the Pd foil, indicating that the Pd is mainly in its metallic state (Figure 2A). The intensity of the metallic peak at ∼24.39 keV, however, shows a slight decrease. In addition, a small feature at ∼24.37 keV may indicate the presence of Pd−O species. These changes become more pronounced in Pd/CoO−C. Although the pre-edge line does not display a distinct shift to higher energies, the intensity of the metallic peak decreases significantly. The improvement in the feature at ∼24.37 keV is more significant, implying a high content of Pd−O species. These phenomena suggest the maintenance of the metallic features in Pd/NiO−C and Pd/CoO−C and also the appearance of the Pd−O component accompanied by a concomitant suppression of the Pd^0 contribution, in particular, for Pd/CoO−C.

Comparing the Fourier transformed k_2-weighted Pd *K*-edge EXAFS spectrum for Pd/NiO−C with the Pd foil reference reveals that the Pd nanoparticles are almost completely metallic, in good agreement with the XANES and XPS results (Figure 2B). The relative intensity of the feature at ∼2.5 Å

DOI: 10.1021/cs501356h
ACS Catal. 2015, 5, 575−586

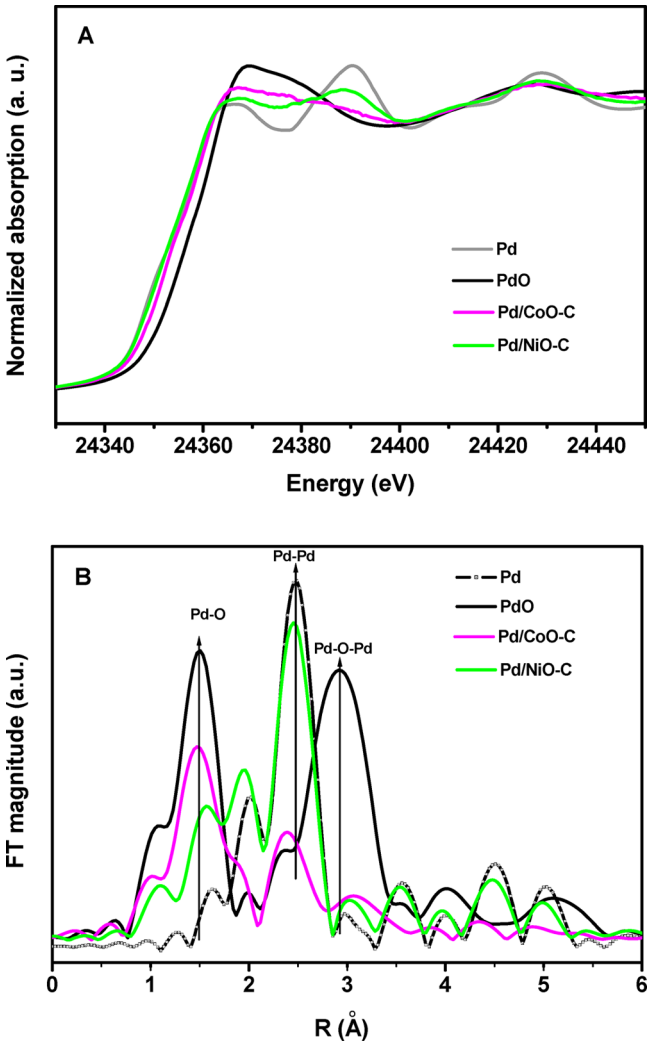

Figure 2. (A) Pd *K*-edge XANES spectra and (B) Fourier transform of Pd *K*-edge EXAFS spectra for the Pd/Co−C and Pd/NiO−C samples and Pd foil and PdO references.

(phase uncorrected) is slightly smaller than the reference peak, hinting at the presence of an overlapping additional scattering pair at a shorter distance than Pd−Pd.[40] A more pronounced reduction in the intensity is observed for Pd/CoO−C. In addition, none of the characteristic features of Pd oxide at ∼1.5 and 2.9 Å (phase uncorrected) is detected. Therefore, the second component can be attributed to a Pd−O signal with a low *Z* scatterer.[40] The EXAFS data were then fitted with two theoretical contributions: one originating from Pd in a metallic environment (Pd−Pd) and a second component corresponding to Pd−O (Table 1). A Pd−Pd coordination number of 6.8 ± 1.1 and a bond distance of 2.73 ± 0.01 Å were obtained for Pd/NiO−C. The under-coordination relative to the bulk metal can be explained by the formation of Pd−O, which decreases the coordination number; the Pd−O coordination number in bulk PdO is 4.3. Indeed, a small Pd−O contribution appears in Pd/NiO−C, with a coordination number of 1.9. The first nearest neighbor Pd−Pd coordination number dramatically decreases to 2.1 ± 0.8 in Pd/CoO−C, while the Pd−O coordination number increases to 3.6 ± 0.7. These phenomena may be related to the formation of very small three-atom Pd clusters, as well as to the formation of Pd−O.[41] The Pd−Pd distance is reduced to 2.71 ± 0.01 Å. The shorter length of the Pd−Pd bond, reduced by approximately 0.07 nm compared with bulk Pd (2.78 ± 0.01 Å), also supports the formation of finely dispersed Pd clusters.[42]

The Pd−O contribution, however, cannot be simply attributed to the formation of Pd−O bonds in a palladium oxide phase.[40b,43] The XANES spectrum does not exhibit the white-line feature characteristic of PdO, and the Pd−O−Pd coordination in palladium oxide is insignificant in the FT-EXAFS spectra of both Pd/CoO−C and Pd/NiO−C. In addition, the Pd−O bond in the Pd/CoO−C (0.210 nm) and Pd/NiO−C (0.208 nm) samples is longer than the covalent Pd−O bond (0.202 nm) in PdO. A previous study showed that long metal−O interaction distances between atoms within nanoparticles in contact with O from an underlying oxide support or from a zeolite were observed under H_2 treatment.[39a,41] The preferential formation of Pd−O at the nanoparticle−oxide interface rather than on the outer particle surface has also been observed on Pd/Fe_3O_4 by Libuda and co-workers.[38] As a result, we assume that the highly dispersed Pd_x clusters are intercalated with the CoO-containing support and strongly interact with transition metal oxide to form Pd−O bonds instead of palladium oxides.

HRSEM images for the NiO−C carrier show ordered mesopore arrays and the confinement of nanoparticles approximately ∼9.0 nm in diameter within the pore walls (Figure 3A). To confirm that the particles are embedded inside the matrix, dark-field SEM images were taken from the same domain (Figure 3B). Many well-dispersed, uniform nanoparticles are observed, indicating the intercalation of the oxide nanoparticles. Particle aggregation outside the carbon mesostructure can be excluded, indicating the restriction of phase separation between NiO and support upon heating. After the Pd nanoparticles are loaded, the hexagonally arranged pores

Table 1. Fit Parameters of Pd *K*-Edge EXAFS Spectra for the Pd/CoO−C and Pd/NiO−C Samples and the Pd and PdO References

sample	shell	N^a	R (Å)^b	σ^2 ($\times 10^{-3}$ Å^2)^c	ΔE_0 (eV)^d
Pd/CoO−C	Pd−O	3.6 ± 0.7	2.10 ± 0.01	5.2 ± 2.6	2.1
	Pd−Pd	2.1 ± 0.8	2.71 ± 0.01	4.2 ± 2.3	−6.6
Pd/NiO−C	Pd−O	1.9 ± 0.5	2.08 ± 0.01	6.0	3.0
	Pd−Pd	6.8 ± 1.1	2.73 ± 0.01	5.7 ± 1.0	−7.6
Pd	Pd−Pd	12.4 ± 1.4	2.78 ± 0.01	8.4 ± 1.3	−7.0
PdO	Pd−O	4.3 ± 0.3	2.02 ± 0.01	1.3 ± 0.7	−3.2
	Pd−Pd	4.6 ± 0.6	3.03 ± 0.01	4.4 ± 0.8	−7.2
	Pd−Pd	7.7 ± 1.1	3.42 ± 0.01	4.4 ± 0.8	−7.2

^{a}Coordination number. ^{b}Distance between absorber and backscatterer atoms. ^{c}Debye−Waller factor. ^{d}Inner potential correction.

DOI: 10.1021/cs501356h
ACS Catal. 2015, 5, 575−586

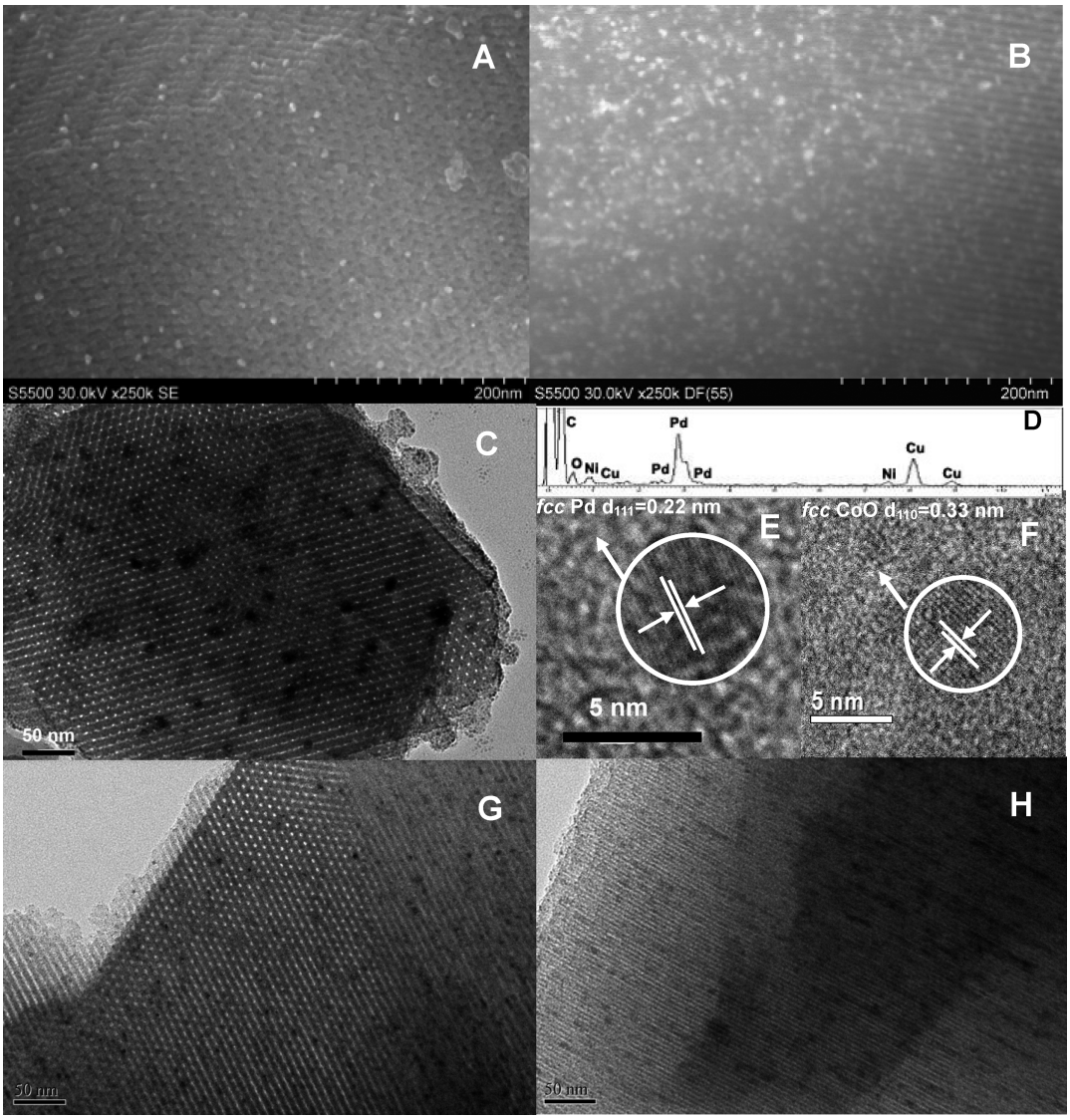

Figure 3. (A) HRSEM, (B) dark-field HRSEM, (C,G,H) TEM, and (E,F) HRTEM images and (D) EDX pattern for the mesoporous carriers and supported palladium catalysts: (A,B) NiO−C; (C−E) fresh Pd/NiO−C; (F,G) fresh Pd/CoO−C; and (H) used catalyst Pd/CoO−C-10run. The images (A) and (B) are taken from the same domain, and (B) is a dark-field SEM image.

and well-dispersed oxide nanoparticles with a size of approximately 9.0 nm are retained (Figure 3C). The EDX pattern reveals the coexistence of Ni and Pd, although the particles of each metal cannot be exclusively identified (Figure 3D). Figure 3E shows a representative particle with a size of 5 nm, revealing the characteristic fcc Pd{111} lattice fringe at 0.22 nm. TEM images for the Pd/CoO−C catalyst show oriented and hexagonally arranged pores, indicating an ordered 2-D hexagonal mesostructure (Figure 3G). Dark dots are highly dispersed inside the whole mesoporous matrix. No large particles can be found, implying the absence of any highly aggregated oxide or palladium particles. The particle shown in Figure 3F, which is approximately 5 nm in size with a *d* spacing value of 0.33 nm, can be attributed to the {110} lattice of CoO.[44] The resolution of the Pd nanoparticles is difficult to determine, possibly due to the extremely small dimensions of the Pd clusters. In fact, a rather diffused diffraction peak at approximately 40° is detected in the wide-angle XRD pattern that overlaps with the CoO peaks, implying the existence of relatively small palladium nanoparticles (SI Figure S7).

CO chemisorption measurements were used to calculate the size of the metallic Pd particles (Table 2). The palladium particle sizes corresponding to the Pd/CoC−C < Pd/MC <

Table 2. Structural and Textural Parameters of the Supports, Freshly Supported Palladium Catalysts after Reduction in Forming Gas, and the Catalyst after 10 Catalytic Runs in the Suzuki Reaction

catalyst	d_{Pd}[a] (nm)	a_0 (nm)	S_{BET} (m^2/g)	V_t (cm^3/g)	D_p (nm)
CoO−C		9.3	591	0.43	3.3
Pd/CoO−C	1.3	9.3	504	0.38	3.0
Pd/CoO−C-10run[b]	1.5	9.3	499	0.37	3.0
NiO−C		10.1	521	0.42	4.1
Pd/NiO−C	5.4	9.9	446	0.42	4.1
MC		9.5	515	0.36	3.0
Pd/MC	1.9	9.5	418	0.32	3.0

[a]Particle size, calculated from the CO chemisorption. [b]Pd/CoO−C catalyst after 10 catalytic runs.

DOI: 10.1021/cs501356h
ACS Catal. 2015, 5, 575−586

Pd/NiO−C series are 1.3, 1.9, and 5.4 nm, respectively, in good agreement with TEM imaging and XAFS results.

Representative diffraction peaks in the small-angle range attributed to the two-dimensional (2-D) hexagonal mesostructure are observed for all of the mesoporous carriers and catalysts (Figure 4), especially one strong (100) diffraction peak at 2θ = 0.5−1.5° and two weak peaks (110 and 200) at higher angles. The cell parameters for the supported palladium catalysts are similar to the mesoporous carriers. These results further indicate that the mesoporous oxide−carbon composites are stable, and the highly ordered mesostructure is retained after impregnation with metallic solution and the subsequent drying and reduction steps.[45] The sorption isotherms of the supported palladium catalysts show typical type-IV curves with significant nitrogen uptake at moderate pressures, indicative of uniform mesopores (Figure 5). The supported palladium catalysts over different carriers of CoO−C, NiO−C, and pristine mesoporous carbon show similar BET surface areas (~500 m^2/g) and uniform pore sizes (~3 nm) (Table 2). A comparison of the isotherms of the mesoporous carriers (SI Figure S8) shows that the incorporation of Pd produces minor effects on the pore size, pore volume, and surface area.

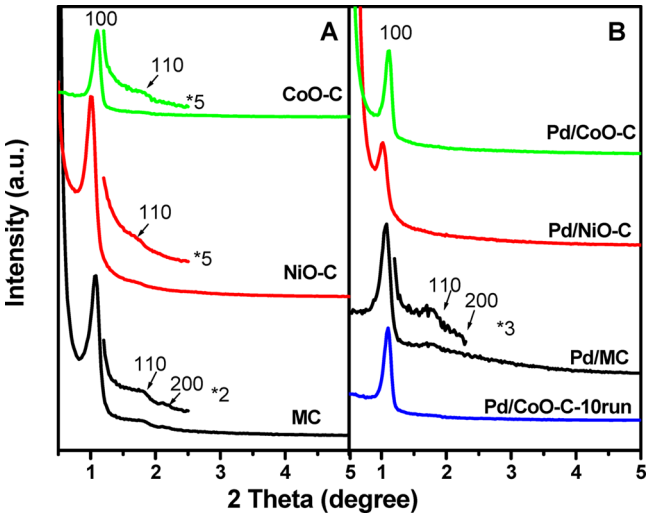

Figure 4. Small-angle patterns for (A) the mesoporous carriers and (B) the supported Pd catalysts. Pd/CoO−C-10run denotes the heterogeneous palladium catalyst after being used to catalyze 10 Suzuki reaction runs.

3.2. Suzuki Coupling Reactions of Chlorobenzene and Phenylboronic Acid in Water. Organic reactions in water have been investigated for use in the chemical and pharmaceutical industries, as they offer the possibility of providing environmentally benign reaction conditions by reducing the burden of organic solvent disposal. The ability to perform the coupling reaction under mild aqueous conditions is highly sought after. The mesoporous supported palladium catalyst Pd/CoO−C was used as a heterogeneous catalyst in Suzuki coupling reactions with water as the solvent and in air at 80 °C for the synthesis of biphenyls (Figure 6). The catalyst exhibited a relatively high conversion of chlorobenzene (49%, 8 h) and selectivity (>98%) to biphenyl, indicating its ability to activate aryl chlorides under the organic solvent-free, ligand-free, and phase-transfer catalyst-free conditions imposed. The initial reaction rate and TON value were calculated to be approximately 11 mmol·mmol(Pd)$^{-1}$ h^{-1} and 49, respectively. The controlled reactions included the homocoupling of either chlorobenzene or phenylboronic acid under the same conditions. Undetectable and less than 4% biphenyl can be found in the coupling reactions of chlorobenzene or phenylboronic acid, respectively. As a result,

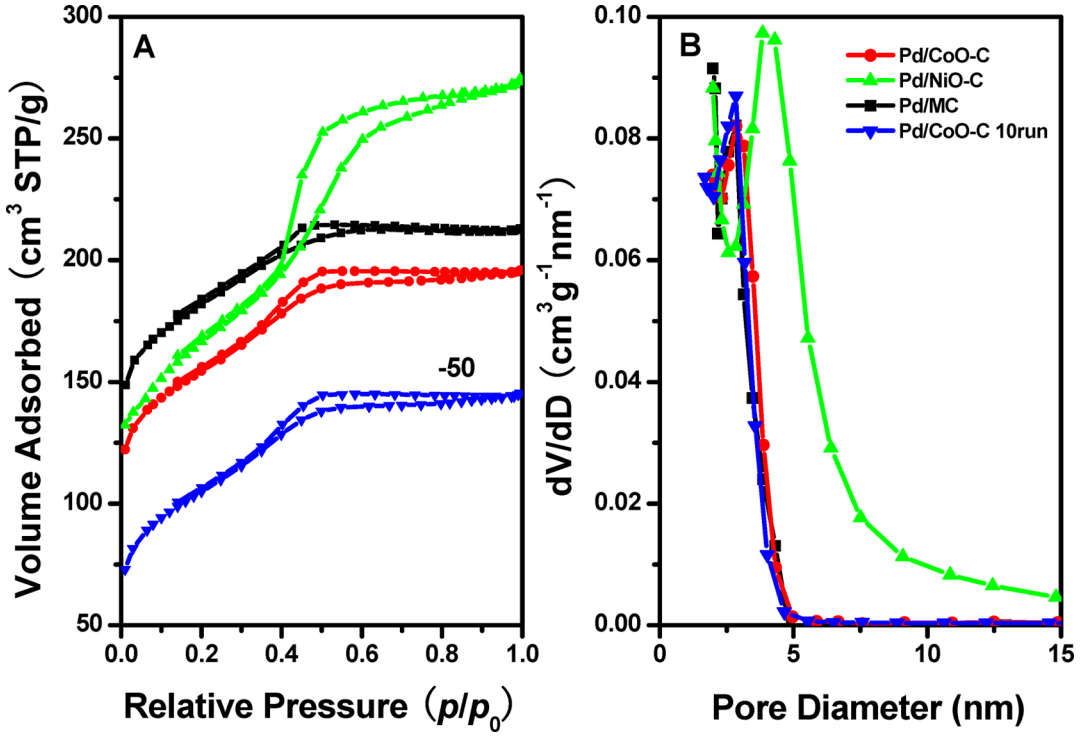

Figure 5. (A) Nitrogen sorption isotherms and (B) pore size distribution curves of the freshly mesoporous supported palladium catalysts and the used Pd/CoO−C-10run catalyst after 10 catalytic runs. The isotherms of Pd/CoO−C-10run are offset vertically by minus 50 cm^3/g.

DOI: 10.1021/cs501356h
ACS Catal. 2015, 5, 575−586

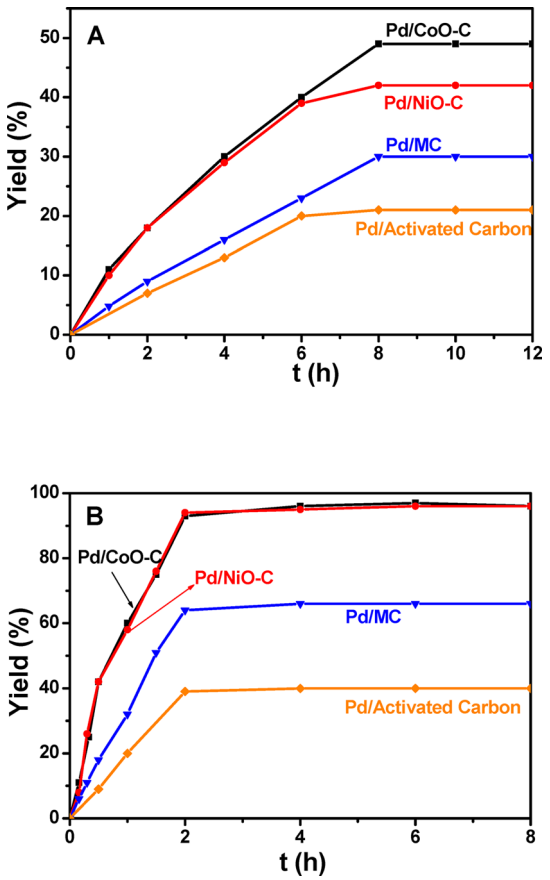

Figure 6. Time conversion plots for the Suzuki reaction of (A) chlorobenzene (1 mmol) and (B) bromobenzene (1 mmol), phenylboronic acid (1.2 mmol), and sodium carbonate (2 mmol) in water at 80 °C over the supported palladium catalysts (0.01 mmol Pd for mesoporous catalyst and 0.017 mmol Pd for the activated carbon supported catalyst).

most biphenyl is originated from the cross-coupling, although we cannot completely exclude the reductive homocoupling of chlorobenzene and oxidative homocoupling of phenylboronic acid. A conversion plateau occurs within 8 h. The reused Pd/CoO−C catalyst after hot infiltration exhibits an initial reaction rate of 10.5 mmol·mmol(Pd)$^{-1}$ h^{-1}, similar to the fresh one. Thus, the product inhibition may be responsible for the suppression of the reaction. When bromobenzene was used as a reactant, approximately 96% of it was converted to product within 6 h, and the initial reaction rate increased to 75 mmol·mmol(Pd)$^{-1}$ h^{-1}. The different initial reaction rates imply the difficult activation of the C−Cl bond.

The high activity for the Suzuki coupling reaction of aryl borides or aryl iodides has also been observed for other Pd-containing heterogeneous catalysts, such as Pd/MCM-41,[46] Pd/MgO,[47] Pd/PdO/Cu,[48] and Pd/activated carbon.[49] There have only been a few reports using Pd(0)-based heterogeneous catalysts to catalyze the Suzuki coupling reaction of chlorobenzene, and almost all cases employed organic solvents, such as DMF and DMA, and the additive of TBAB; in addition, sometimes harsh conditions, such as temperatures as high as 200 °C (SI Table S1), were employed.[13b,17,50] The promoting role of TBAB is distinct. A much lower conversion of chlorobenzene has been shown to be obtained in the absence of TBAB.[50c] As mentioned above, the stabilization of Pd colloids and complexes by TBAB cannot be completely excluded.[7] Soluble Pd colloids and complexes may contribute to the activity.[51,52] In fact, Sowa and co-workers postulated that the oxidative addition step produces an Ar−Pd(II)−X species, which desorbs from the charcoal support.[21a] After the transmetalation step, the soluble palladium species precipitate onto the support, and the system cools down. This interesting observation has been described as the "boomerang effect" or dissolution−redeposition mechanism.[19,34b,53,54] Köhler and co-workers investigated the dissolution−redeposition mechanism over a solid-supported Pd nanoparticles during Suzuki coupling reaction in water even under a mild condition of 65 °C.[19] A substantial amount of Pd leaching (up to 50%) from Pd/Al_2O_3 can be detected during the reaction which is enhanced by TBAB,[19] and the aryl bromide conversion is highly related to the Pd leaching. Dissolved Pd is deposited onto the support at the end of the reaction.[54]

The hot filtration test has been considered a strong test for assessing the presence of soluble active palladium. In this procedure, solid catalysts are filtered out of the reaction, and the filtrate is monitored for continued activity.[55] When Pd/CoO−C is hot filtered, after approximately 44% conversion, the filtrate loses its activity, which is proof of a heterogeneous catalysis (Figure 7). However, this interpretation shows certain

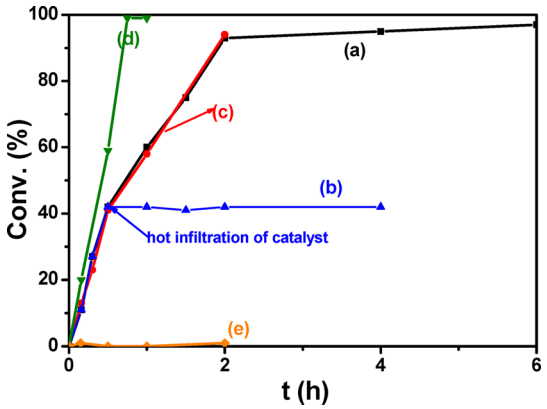

Figure 7. Plots of bromobenzene conversion with either palladium acetate or Pd/CoO−C as catalyst: (a) Pd/CoO−C activity without any poisoning agent, (b) cessation of Pd/CoO−C activity upon hot filtration of the catalyst after 30 min reaction, (c) Pd/CoO−C activity in the presence of mercapto-functionalized mesoporous silica SH-SBA-15 trapping agent with a SH:Pd of 35, (d) control reaction using palladium acetate as catalyst in the presence of TBAB without any poison, and (e) cessation of palladium acetate activity by adding SH-SBA-15 at start of reaction. Reaction conditions: 0.01 mmol Pd, 1 mmol aryl bromide, 1.2 mmol phenylboronic acid, 2 mmol K_2CO_3, 10 mL water, 80 °C.

limitations, especially for palladium-catalyzed reactions, when other tests are not used to support the conclusions.[43,51] The (local) concentration of Pd leached may be continuously low, and Heck and Suzuki reactions can be catalyzed by extremely small amounts of palladium (as low as 0.00001%).[56] Furthermore, Pd species can first dissolve in solution as a function of time correlated to conversion and then redeposit on the solid as mentioned above.[19,54] These phenomena can lead to the incorrect conclusion that no active soluble catalytic species were present before filtration.[51] Therefore, other tests are needed to verify whether heterogeneous catalysis is indeed occurring.[33]

DOI: 10.1021/cs501356h
ACS Catal. 2015, 5, 575−586

Comparisons of the activities of soluble palladium acetate and immobilized Pd nanoparticles on mesoporous CoO−C are displayed in Figure 7. The reaction using soluble palladium acetate in the presence of TBAB begins rapidly, with an initial reaction rate (20 mmol·mmol(Pd)$^{-1}$ h^{-1}) much higher than that of Pd/CoO−C. Subsequently, we investigated the use of thiol-functionalized mesoporous silicate SH-SBA-15 to distinguish homogeneous and heterogeneous contributions to catalysis. SH-SBA-15 has been postulated to be an effective and selective poison of homogeneous palladium species and can therefore be used as a test for the heterogeneity of palladium catalysts developed for the Heck and Suzuki reactions.[33] The SH/Pd ratio is approximately 35, with a sufficiently high local sulfur concentration arising from the bound thiols such that captured palladium is rapidly overcoordinated by neighboring thiols before it can be released back into solution.[33] In our study, the complete quenching of catalysis by palladium acetate that is observed upon the addition of the poison is similar to literature reports, demonstrating the successful capture of soluble palladium species by SH-SBA-15.[33] In contrast, an indistinct change in the conversion plot in the presence of thiol groups is detected in Pd/CoO−C catalysis, excluding the possibility that the activity is due to soluble Pd in liquid phase (Figure 7).[57]

Different aryl halides were also used as substrates (Table 3). A high yield of approximately 90% can be achieved for the

Table 3. Catalytic Performance in the Coupling Reaction for Aryl Chlorides and Bromides over the Pd/CoO−C Catalyst[a]

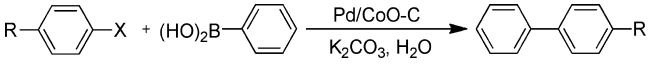

entry	X	R	t (h)	yield (%)
1	Cl	H	8	49
2	Cl	CN	8	94
3	Cl	NO_2	8	88
4	Cl	CH_3	24	29
5	Cl	CH_3O	24	19
6	Br	H	4	96
7	Br	OH	8	89
8	Br	COOH	8	97

[a]All Suzuki reactions were performed using 0.03 g of supported palladium catalyst containing 1 mol % of Pd, 1 mmol aryl chlorides or bromide, phenylboronic acid (1.2 mmol), and K_2CO_3 (2 mmol) in 10 mL of water under air at 80 °C.

reaction between phenylboronic acid and aryl chlorides containing electron-withdrawing groups attached to their benzene ring. When electron-donating groups are present, the yields drop significantly but remain at approximately 20%. The product yields are approximately 90% over the Pd/CoO−C catalyst in the coupling reactions of phenylboronic acid and aryl bromides, regardless of the presence of electron-withdrawing or electron-donating groups.

The catalytic performance in the Suzuki coupling reaction of supported palladium catalysts with different pore surface and textural properties was also tested and is described in Figure 6. The ordered mesoporous Pd/NiO−C catalyst displays a lower product yield within 10 h (42%) but a similar initial reaction rate (10 mmol·mmol(Pd)$^{-1}$ h^{-1}) in the Suzuki coupling reaction of chlorobenzene; this catalyst performs similarly to Pd/CoO−C in the conversion of bromobenzene. By comparison, the pristine ordered mesoporous carbon-supported Pd catalyst, in which there are no intercalated transition oxide nanoparticles, shows a reduced reaction rate of 4.8 mmol·mmol(Pd)$^{-1}$ h^{-1} and product yield of 30% after 8 h in the coupling reaction of chlorobenzene and phenylboronic acid, as well as a reduced reaction rate of 37 mmol·mmol(Pd)$^{-1}$ h^{-1} and product yield of 66% after 4 h in the coupling reaction of bromobenzene. A further decrease in catalytic performance is detected for the activated carbon-supported Pd catalyst. This catalyst possesses a high surface area of 1043 m^2/g. The pore size distribution is wide but shows a high proportion of mesopores with a most probable distribution at 4.0 nm (SI Figure S9). The reaction rates are as low as 2.1 and 11 mmol·mmol(Pd)$^{-1}$ h^{-1} in the coupling of chlorobenzene and bromobenzene, respectively.

3.3. Stability of the Catalyst. The time plots for the catalytic conversion of bromobenzene over the recovered Pd/CoO−C catalyst are similar to the time plots obtained over the fresh catalyst (data not shown here). We also tested the conversion of bromobenzene after 1 h in successive runs; the compiled data are shown in Figure 8. No obvious changes are

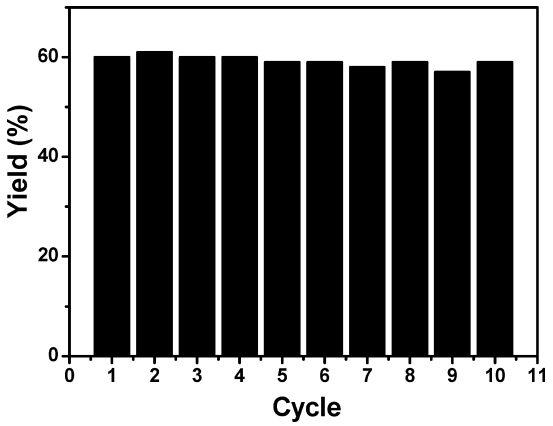

Figure 8. Reusability of the Pd/CoO−C catalyst upon recycling it in the water-mediated Suzuki reaction of bromobenzene and phenylboronic acid.

detected in the catalytic performance after 10 runs, demonstrating that the reused catalyst maintains the reaction rate and conversion. The reaction mother liquors after hot separation of the catalyst after each run were collected and mixed. The Pd content in the final mixture is below the detection limit of ICP-AES analysis, implying that negligible metal leaching occurs during repeated reactions on the same catalyst. These results suggest that the Pd/CoO−C catalyst is stable and reusable.

The XPS spectrum, N_2 sorption isotherms, small-angle XRD, CO chemisorption, and TEM images for the catalyst after 10 runs are shown. The Pd $3d_{5/2}$ region can be qualitatively decomposed into two regions: a low BE component (335.0−335.1 eV) related to metallic Pd and a high BE region (approximately 336.6−336.7 eV) due to Pd atoms in thin oxide layers (Figure 1B).[37] Compared with the fresh catalyst, the signal at the high BE region is slightly stronger, implying an improvement in the Pd−O bond formation during the reaction, possibly due to the interaction between Pd atoms and the O atom in CoO. This phenomenon implies the involvement of coordinated Pd species such as Pd−O in the Suzuki reaction. The TEM image shows the stripe-like pore arrays of the catalyst, containing highly dispersed nanoparticles (Figure 3H).

DOI: 10.1021/cs501356h
ACS Catal. 2015, 5, 575−586

High amounts of aggregation of large nanoparticles cannot be found, demonstrating that the heterogeneous catalyst is stable, and the reaction conditions have only minor effects on the catalyst structure. The particle size for Pd estimated by CO chemisorption analysis is approximately 1.5 nm, similar to the size measured for the fresh catalyst. The XRD pattern and N_2 sorption isotherms further confirm the stability of the catalyst (Figure 4B and Figure 5). The used catalyst exhibits similar structural and textual properties to the fresh one, indicating that the ordered 2-D mesostructure, high surface area, and uniform mesopores of the catalyst are all retained.

4. DISCUSSION

In general, the Suzuki reaction is thought to proceed through three steps: oxidative addition, transmetalation, and reductive elimination.[58] The decreased reactivity of aryl bromides and chlorides in the Pd-catalyzed reaction compared to that of iodobenzene can be attributed to their more difficult oxidative addition to Pd(0). The activation of iodobenzene undergoes an associative or direct mechanism requiring either single or double coordination to Pd.[59] The oxidative addition of bromoarenes appears to occur by a combination of irreversible reactions of the bromoarene with the two-coordinate Pd(0) species and dissociation of the ligand. By comparison, the activation of chlorobenzene requires ligand loss on Pd.[59] Dissociation of the bidentate ligands to singly coordinated ligands occurs on the active catalyst.[60] Therefore, the dissociation of bidentate ligands to a reactive ligand loss intermediate prior to reaction with chloroarene is expected to cleave the less reactive C−Cl bond.

The contribution of soluble Pd species in liquid phase to the performance of the catalyst can be almost entirely excluded. Therefore, the coupling reaction occurs inside the mesopores which have high adsorption capacities for organic substances from water.[61] The enrichment of substrate inside the pores and the enhancement of accessibility of substrates to active Pd sites can improve the reaction to some extent.[20] XAFS data reveal that a fraction of the Pd atoms in the nanoparticles are coordinative unsaturated after immobilization on a transition metal oxide containing carbon support. This result is supported by the decrease in the metallic Pd−Pd scattering intensity and the increase in the intensity of the Pd−O XANES absorption peak, which is accompanied by an increase of the additional Pd−O component (Figure 2A). In addition, a decrease in the Pd−Pd coordination number is observed in parallel with the appearance of Pd−O bonding. The Pd−O contribution can be attributed to the interface Pd−O bonds between Pd_x nanoclusters and the transition metal oxide rather than to a distinct palladium oxide phase, as evidenced by XPS and XAFS results. The driving force for the stabilization of the Pd−O bond can be attributed to the interfacial interaction between Pd and CoO or NiO. This phenomenon is more distinct for the Pd/CoO−C catalyst. The higher fraction of Pd−O in Pd/CoO−C than in Pd/NiO-C may be related to the smaller particle size of the former catalyst, which should lead to a much higher interface atom/surface atom interaction ratio. The unsaturated coordination Pd may be responsible for the activation of chlorobenzene, as was observed previously for Pd on the USY zeolite, on which strong acid sites stabilize surface defect atoms and tune the coordination between Pd and O in zeolite.[9,41] The cleavage of the C−Cl bond is promoted by Pd atoms that have low coordination numbers. In the present case, the leaching Pd species, if any, are assumed to be diffused into the solution due to the large enough mesopores, similar to Pd supported on activated carbon[19] and ordered mesoporous silica SBA-15.[33] An obvious decrease for bromobenzene conversion with addition of SH-SBA-15 suggests the heterogeneous reaction over the Pd clusters supported on CoO−C. However, an assumption that the Pd leaching is restricted inside the pores cannot be completely ruled out. The dissolution and redeposition completely occur inside the pores, and after the reaction, the catalyst can be entirely recovered. A thorough study should be undertaken.

The Pd/CoO−C catalyst possesses the highest product yields and initial reaction rates in the coupling reaction of both bromobenzene and chlorobenzene. Pd/NiO−C exhibits a much higher aryl bromide conversion activity and initial reaction rate, as well as a moderately higher aryl chloride conversion activity and initial reaction rate when compared to Pd/MC. When the conversion of chlorobenzene over the exposed surface Pd atom (turnover frequency, TOF) was considered, Pd/NiO−C with a larger particle size of about 5.4 nm (surface atoms/total atoms faction of about 0.255) exhibits a much higher TOF value than Pd/CoO−C (atomic fraction exposed >0.9). This result may also reflect that the surface coverage of product may inhibit the reaction. The slow reduction elimination step of the product may hinder the reaction rate.

The interface interaction between the catalyst metal and the support oxides through the formation of Pd−O bonds may also facilitate the stabilization of the Pd nanoparticles on carbon, thereby restricting the leaching and aggregation of the metal.

Finally, the uniform mesopores and the hydrophobic feature of the carbon support may also contribute to the high activity of the catalyst by assisting in the transportation of reactants and products during the course of the reaction. In fact, the activated carbon-supported Pd catalyst shows a much lower initial reaction rate and product yield than the mesoporous carbon catalysts.

5. CONCLUSIONS

The interfacial interaction between palladium and CoO can generate small Pd_x clusters with low coordination that are stabilized by the coordination of Pd and O. These clusters can activate chlorobenzene in the water-mediated Suzuki coupling reaction performed in the absence of TBAB and ligands. The transition metal oxide nanoparticles are intercalated into a mesoporous carbon matrix and can catalyze the production of biphenyl in a yield of 49% over Pd/CoO−C. The product yields of the reaction of chlorobenzene derivatives containing electron-withdrawing groups attached to their benzene ring can reach approximately 90%. Negligible Pd leaching is detected either during the reaction, confirmed by thiol-functionalized mesoporous silica trapping, or after reaction, confirmed by hot filtration. The heterogeneous catalyst can be reused with no observable decrease in the initial reaction rate. The TBAB-free and ligand-free conditions, the use of pure water as solvent, and the reusability of the Pd/CoO−C catalyst tested here make this catalyst an attractive material for use in practical applications.

■ ASSOCIATED CONTENT

Supporting Information

The following file is available free of charge on the ACS Publications website at DOI: 10.1021/cs501356h.

DOI: 10.1021/cs501356h
ACS Catal. 2015, 5, 575−586

Preparation of carbon precursors; preparation and characterization of pristine mesoporous silica SBA-15 and thiol-functionalized mesoporous silica SH-SBA-15, including XPS spectra, elemental analysis, TG curves in air, FT-IR spectra, XRD patterns, and N_2 sorption isotherms; XRD patterns and N_2 sorption isotherms of carriers and supported Pd catalysts; and Suzuki coupling of aryl chlorides and phenylboronic acid catalyzed by different palladium catalysts (PDF)

AUTHOR INFORMATION

Corresponding Author

*Tel: 86-21-6432-2516. Fax: 86-21-6432-2511. E-mail: ywan@shnu.edu.cn.

Notes

The authors declare no competing financial interest.

ACKNOWLEDGMENTS

This work was supported by State Key Basic Research Program of China (2013CB934102), the NSF of China (21322308 and 21173149), the Ministry of Education of China (PCSIRT-IRT1269 and 20123127110004), the International Joint Laboratory on Resource Chemistry (IJLRC), and the Shanghai Sci. & Tech. and Edu. Committee (11JC1409200, DZL123 and S30406).

REFERENCES

(1) Yin, L.; Liebscher, J. *Chem. Rev.* **2007**, *107*, 133−173.

(2) (a) Walvoord, R. R.; Kozlowski, M. C. *J. Org. Chem.* **2013**, *78*, 8859−8864. (b) Balanta, A.; Godard, C.; Claver, C. *Chem. Soc. Rev.* **2011**, *40*, 4973−4985.

(3) (a) Grushin, V. V.; Alper, H. *Chem. Rev.* **1994**, *94*, 1047−1062. (b) Littke, A. F.; Fu, G. C. *Angew. Chem., Int. Ed.* **2002**, *41*, 4176−4211. (c) Yuan, B.; Pan, Y.; Li, Y.; Yin, B.; Jiang, H. *Angew. Chem., Int. Ed.* **2010**, *49*, 4054−4058. (d) Jin, M.-J.; Lee, D.-H. *Angew. Chem., Int. Ed.* **2010**, *49*, 1119−1122. (e) Sau, S. C.; Santra, S.; Sen, T. K.; Mandal, S. K.; Koley, D. *Chem. Commun.* **2012**, *48*, 555−557.

(4) Bedford, R. B.; Cazin, C. S. J.; Holder, D. *Coord. Chem. Rev.* **2004**, *248*, 2283−2321.

(5) Barnard, C. *Platinum Met. Rev.* **2008**, *52*, 38−45.

(6) (a) Barder, T. E.; Walker, S. D.; Martinelli, J. R.; Buchwald, S. L. *J. Am. Chem. Soc.* **2005**, *127*, 4685−4696. (b) Gstöttmayr, C. W. K.; Böhm, V. P. W.; Herdtweck, E.; Grosche, M.; Herrmann, W. A. *Angew. Chem., Int. Ed.* **2002**, *41*, 1363−1365. (c) Dupont, J.; Consorti, C. S.; Spencer, J. *Chem. Rev.* **2005**, *105*, 2527−2572.

(7) Felpin, F.-X.; Ayad, T.; Mitra, S. *Eur. J. Org. Chem.* **2006**, *2006*, 2679−2690.

(8) (a) Jana, S.; Haldar, S.; Koner, S. *Tetrahedron. Lett.* **2009**, *50*, 4820−4823. (b) Ungureanu, S.; Deleuze, H.; Babot, O.; Achard, M. F.; Sanchez, C.; Popa, M. I.; Backov, R. *Appl. Catal., A* **2010**, *390*, 51−58.

(9) Okumura, K.; Tomiyama, T.; Okuda, S.; Yoshida, H.; Niwa, M. *J. Catal.* **2010**, *273*, 156−166.

(10) Zhang, P.-P.; Zhang, X.-X.; Sun, H.-X.; Liu, R.-H.; Wang, B.; Lin, Y.-H. *Tetrahedron. Lett.* **2009**, *50*, 4455−4458.

(11) Scheuermann, G. M.; Rumi, L.; Steurer, P.; Bannwarth, W.; Mülhaupt, . *J. Am. Chem. Soc.* **2009**, *131*, 8262−8270.

(12) Gallon, B. J.; Kojima, R. W.; Kaner, R. B.; Diaconescu, P. L. *Angew. Chem., Int. Ed.* **2007**, *46*, 7251−7254.

(13) (a) Llabrés i Xamena, F. X.; Abad, A.; Corma, A.; Garcia, H. *J. Catal.* **2007**, *250*, 294−298. (b) Saha, D.; Sen, R.; Maity, T.; Koner, S. *Langmuir* **2013**, *29*, 3140−3151.

(14) (a) Choudary, B. M.; Madhi, S.; Chowdari, N. S.; Kantam, M. L.; Sreedhar, B. *J. Am. Chem. Soc.* **2002**, *124*, 14127−14136. (b) Lakshmi Kantam, M.; Roy, S.; Roy, M.; Sreedhar, B.; Choudary, B. M. *Adv. Synth. Catal.* **2005**, *347*, 2002−2008.

(15) Ravat, V.; Nongwe, I.; Meijboom, R.; Bepete, G.; Coville, N. J. *J. Catal.* **2013**, *305*, 36−45.

(16) Marck, G.; Villiger, A.; Buchecker, R. *Tetrahedron. Lett.* **1994**, *35*, 3277−3280.

(17) LeBlond, C. R.; Andrews, A. T.; Sun, Y.; Sowa, J. R. *Org. Lett.* **2001**, *3*, 1555−1557.

(18) (a) Lysén, M.; Köhler, K. *Synlett* **2005**, *11*, 1671−1674. (b) Lysén, M.; Köhler, K. *Synthesis* **2006**, *4*, 692−698.

(19) Soomro, S. S.; Ansari, F. L.; Chatziapostolou, K.; Köhler, K. *J. Catal.* **2010**, *273*, 138−146.

(20) Soomro, S. S.; Röhlich, C.; Köhler, K. *Adv. Synth. Catal.* **2011**, *353*, 767−775.

(21) (a) Conlon, D. A.; Pipik, B.; Ferdinand, S.; LeBlond, C. R.; Sowa, J. R.; Izzo, B.; Collins, P.; Ho, G.-J.; Williams, J. M.; Shi, Y.-J.; Sun, Y. *Adv. Synth. Catal.* **2003**, *345*, 931−935. (b) Webb, J. D.; MacQuarrie, S.; McEleney, K.; Crudden, C. M. *J. Catal.* **2007**, *252*, 97−109.

(22) (a) Fihri, A.; Bouhrara, M.; Nekoueishahraki, B.; Basset, J.-M.; Polshettiwar, V. *Chem. Soc. Rev.* **2011**, *40*, 5181−5203. (b) Li, X.-H.; Baar, M.; Blechert, S.; Antonietti, M. *Sci. Rep.* **2013**, *3*, 1743.

(23) Stenehjem, E. D.; Ziatdinov, V. R.; Stack, T. D. P.; Chidsey, C. E. D. *J. Am. Chem. Soc.* **2013**, *135*, 1110−1116.

(24) Wan, Y.; Wang, H.; Zhao, Q.; Klingstedt, M.; Terasaki, O.; Zhao, D. *J. Am. Chem. Soc.* **2009**, *131*, 4541−4550.

(25) Wang, W.; Wang, H.-Y.; Wei, W.; Xiao, Z.-G.; Wan, Y. *Chem.—Eur. J.* **2011**, *17*, 13461−13472.

(26) Kong, L.; Wei, W.; Zhao, Q.; Wang, J.-Q.; Wan, Y. *ACS Catal.* **2012**, *2*, 2577−2586.

(27) Meng, Y.; Gu, D.; Zhang, F.; Shi, Y.; Yang, H.; Li, Z.; Yu, C.; Tu, B.; Zhao, D. *Angew. Chem., Int. Ed.* **2005**, *44*, 7053−7059.

(28) Wang, S. Y.; Moon, S. H.; Vannice, M. A. *J. Catal.* **1981**, *71*, 167−174.

(29) Newville, M. *J. Synchrotron. Radiat.* **2001**, *8*, 322−324.

(30) Rehr, J. J.; Albers, R. C. *Rev. Mod. Phys.* **2000**, *72*, 621−654.

(31) (a) Corma, A.; Das, D.; García, H.; Leyva, A. *J. Catal.* **2005**, *229*, 322−331. (b) Polshettiwar, V.; Molnár, Á. *Tetrahedron* **2007**, *63*, 6949−6976.

(32) Della Pina, C.; Falletta, E.; Rossi, M.; Sacco, A. *J. Catal.* **2009**, *263*, 92−97.

(33) Richardson, J. M.; Jones, C. W. *J. Catal.* **2007**, *251*, 80−93.

(34) (a) Kim, K. S. *Phys. Rev. B* **1975**, *11*, 2177−2185. (b) Brundle, C. R.; Chuang, T. J.; Rice, D. W. *Surf. Sci.* **1976**, *60*, 286−300. (c) Tan, B. J.; Klabunde, K. J.; Sherwood, P. M. A. *J. Am. Chem. Soc.* **1991**, *113*, 855−861.

(35) (a) Shen, Z. X.; Allen, J. W.; Lindberg, P. A. P.; Dessau, D. S.; Wells, B. O.; Borg, A.; Ellis, W.; Kang, J. S.; Oh, S. J.; Lindau, I.; Spicer, W. E. *Phys. Rev. B* **1990**, *42*, 1817−1828. (b) Ghosh, M.; Sampathkumaran, E. V.; Rao, C. N. R. *Chem. Mater.* **2005**, *17*, 2348−2352.

(36) Zhao, Y.; Jia, L.; Medrano, J. A.; Ross, J. R. H.; Lefferts, L. *ACS Catal.* **2013**, *3*, 2341−2352.

(37) Semagina, N.; Renken, A.; Laub, D.; Kiwi-Minsker, L. *J. Catal.* **2007**, *246*, 308−314.

(38) Schalow, T.; Laurin, M.; Brandt, B.; Schauermann, S.; Guimond, S.; Kuhlenbeck, H.; Starr, D. E.; Shaikhutdinov, S. K.; Libuda, J.; Freund, H.-J. *Angew. Chem., Int. Ed.* **2005**, *44*, 7601−7605.

(39) (a) Koningsberger, D. C.; Gates, B. C. *Catal. Lett.* **1992**, *14*, 271−277. (b) Hayek, K.; Kramer, R.; Paál, Z. *Appl. Catal., A* **1997**, *162*, 1−15.

(40) (a) Okumura, K.; Niwa, M. *J. Phys. Chem. B* **2000**, *104*, 9670−9675. (b) Paredis, K.; Ono, L. K.; Behafarid, F.; Zhang, Z.; Yang, J. C.; Frenkel, A. I.; Cuenya, B. R. *J. Am. Chem. Soc.* **2011**, *133*, 13455−13464.

(41) Okumura, K.; Matsui, H.; Tomiyama, T.; Sanada, T.; Honma, T.; Hirayama, S.; Niwa, M. *ChemPhysChem* **2009**, *10*, 3265−3272.

(42) Yudanov, I. V.; Metzner, M.; Genest, A.; Rösch, N. *J. Phys. Chem. C* **2008**, *112*, 20269−20275.

(43) Keating, J.; Sankar, G.; Hyde, T. I.; Kohara, S.; Ohara, K. *Phys. Chem. Chem. Phys.* **2013**, *15*, 8555−8565.

DOI: 10.1021/cs501356h
ACS Catal. 2015, 5, 575−586

(44) Liu, J. F.; He, Y.; Chen, W.; Zhang, G. Q.; Zeng, Y. W.; Kikegawa, T.; Jiang, J. Z. *J. Phys. Chem. C* **2007**, *111*, 2−5.
(45) Sakamoto, Y.; Fukuoka, A.; Higuchi, T.; Shimomura, N.; Inagaki, S.; Ichikawa, M. *J. Phys. Chem. B* **2004**, *108*, 853−858.
(46) Gannouni, A.; Rozanska, X.; Albela, B.; Saïd Zina, M.; Delbecq, F.; Bonneviot, L.; Ghorbel, A. *J. Catal.* **2012**, *289*, 227−237.
(47) Dumbre, D. K.; Yadav, P. N.; Bhargava, S. K.; Choudhary, V. R. *J. Catal.* **2013**, *301*, 134−140.
(48) Korzec, M.; Bartczak, P.; Niemczyk, A.; Szade, J.; Kapkowski, M.; Zenderowska, P.; Balin, K.; Lelątko, J.; Polanski, J. *J. Catal.* **2014**, *313*, 1−8.
(49) Narayanan, R.; El-Sayed, M. A. *J. Catal.* **2005**, *234*, 348−355.
(50) (a) Köhler, K.; Heidenreich, R. G.; Krauter, J. G. E.; Pietsch, J. *Chem.—Eur. J.* **2002**, *8*, 622−631. (b) Böhm, V. P. W.; Herrmann, W. A. *Chem.—Eur. J.* **2000**, *6*, 1017−1025. (c) Herrmann, W. A.; Böhm, V. P. W. *J. Organomet. Chem.* **1999**, *572*, 141−145. (d) Jana, S.; Haldar, S.; Koner, S. *Tetrahedron Lett.* **2009**, *50*, 4820−4823. (e) Yang, H.; Han, X.; Ma, Z.; Wang, R.; Liu, J.; Ji, X. *Green Chem.* **2010**, *12*, 441−451. (f) Calò, V.; Nacci, A.; Monopoli, A.; Montingelli, F. *J. Org. Chem.* **2005**, *70*, 6040−6044. (g) Zhang, L.; Su, Z.; Jiang, F.; Zhou, Y.; Xu, W.; Hong, M. *Tetrahedron.* **2013**, *69*, 9237−9244. (h) Artok, L.; Bulut, H. *Tetrahedron Lett.* **2004**, *45*, 3881−3884. (i) Bhunia, S.; Sen, R.; Koner, S. *Inorg. Chim. Acta* **2010**, *363*, 3993−3999. (j) Islam, M.; Mondal, P.; Roy, A. S.; Tuhina, K. *Transition Met. Chem.* **2010**, *35*, 491. (k) Tyrrell, E.; Whiteman, L.; Williams, N. *J. Organomet. Chem.* **2011**, *696*, 3465−3472. (l) Arvela, R. K.; Leadbeater, N. E. *Org. Lett.* **2005**, *7*, 2101−2104.
(51) Köhler, K.; Kleist, W.; Pröckl, S. S. *Inorg. Chem.* **2007**, *46*, 1876−1883.
(52) Reimann, S.; Stötzel, J.; Frahm, R.; Kleist, W.; Grunwaldt, J.-D.; Baiker, A. *J. Am. Chem. Soc.* **2011**, *133*, 3921−3930.
(53) (a) Davies, I. W.; Matty, L.; Hughes, D. L.; Reider, P. J. *J. Am. Chem. Soc.* **2001**, *123*, 10139−10140. (b) Lipshutz, B. H.; Tasler, S.; Chrisman, W.; Spliethoff, B.; Tesche, B. *J. Org. Chem.* **2003**, *68*, 1177−1189.
(54) (a) MacQuarrie, S.; Horton, J. H.; Barnes, J.; McEleney, K.; Loock, H.-P.; Crudden, C. M. *Angew. Chem., Int. Ed.* **2008**, *47*, 3279−3282. (b) Köhler, K.; Heidenreich, R. G.; Soomro, S. S.; Pröckl, S. S. *Adv. Synth. Catal.* **2008**, *350*, 2930−2936.
(55) Sheldon, R. A.; Wallau, M.; Arends, I. W. C. E.; Schuchardt, U. *Acc. Chem. Res.* **1998**, *31*, 485−493.
(56) (a) Phan, N. T. S.; Van Der Sluys, M.; Jones, C. W. *Adv. Synth. Catal.* **2006**, *348*, 609−679. (b) de Vries, A. H. M.; Mulders, J. M. C. A.; Mommers, J. H. M.; Henderickx, H. J. W.; de Vries, J. G. *Org. Lett.* **2003**, *5*, 3285−3288.
(57) Ellis, P. J.; Fairlamb, I. J. S.; Hackett, S. F. J.; Wilson, K.; Lee, A. F. *Angew. Chem., Int. Ed.* **2010**, *49*, 1820−1824.
(58) Miyaura, N.; Suzuki, A. *Chem. Rev.* **1995**, *95*, 2457−2483.
(59) Barrios-Landeros, F.; Carrow, B. P.; Hartwig, J. F. *J. Am. Chem. Soc.* **2009**, *131*, 8141−8154.
(60) Stambuli, J. P.; Bühl, M.; Hartwig, J. F. *J. Am. Chem. Soc.* **2002**, *124*, 9346−9347.
(61) Zhuang, X.; Wan, Y.; Feng, C.; Shen, Y.; Zhao, D. *Chem. Mater.* **2009**, *21*, 706−716.

DOI: 10.1021/cs501356h
ACS Catal. 2015, 5, 575−586